SAND2018-10721C

Nonlinear Ultrasonic Technique for the Quantification of Dislocation Density in Additive Materials

Aurelio Bellotti[1, a)], Jin-Yeon Kim[2] , Joseph E. Bishop[3], Bradley H. Jared[3], Donald Susan[3], Laurence J. Jacobs[1, 2]

[1]*G.W. Woodruff School of Mechanical Engineering, Georgia Institute of Technology, Atlanta, Georgia 30332, USA*
[2] *School of Civil and Environmental Engineering, Georgia Institute of Technology, Atlanta, Georgia 30332, USA*
[3]*Sandia National Laboratories, Albuquerque, New Mexico 87185, USA*

[a)]Corresponding author: aurelio.bellotti@gatech.edu

Abstract. This research applies nonlinear ultrasonic techniques for the quantitative characterization of additively manufactured materials. The characterization focuses on identifying the dislocation density produced during the additive constructive process in order to increase confidence on a part's performance and the success of the manufacturing process. Second harmonic generation techniques based on the transmission of Rayleigh surface waves are used to measure the ultrasonic nonlinearity parameter, β, which has proven a quantitative indicator of dislocations but has not been fully proven in additive manufactured materials. 316L and 304L stainless steel parts made from Powder Bed Fusion and Laser Engineered Net Shaping are compared between AM techniques and with wrought manufactured counterparts. β is consistently higher for additive manufactured parts. An annealing heat treatment is applied to each specimen to reduce dislocation density. β expectedly decreases by annealing in all specimens. A linear ultrasonic measurement is made to evaluate the effectiveness of using nonlinear techniques. The ultrasonic attenuation is higher for additive manufactured parts and increases at higher frequencies.

INTRODUCTION

Additive manufacturing (AM) technology has been developed over the course of a century, but recent advancements have led to a sharp increase in interest. AM allows for the freedom to manufacture complex structures quickly and is valuable for prototyping and making small batch parts. Additional benefits of AM include the ability to manufacture complex internal geometries to tailor specific properties and behaviors of a part [1]. AM methods can be used for a variety of materials, including metals used in highly critical scenarios in the energy and defense industry. Complete adoption in these critical industries is limited by the uncertainty in a part's performance and life cycle. AM materials are subject to variations during the printing process including the print rate, bulk material properties, and cooling rates. Large temperature gradients are formed between the inputted thermal energy needed for the printing process and the remaining structure. Heat is transferred out of a build object through three means: heat dissipates through the build plate, through convection at the top layer and radially through the surrounding environment [2]. The high temperature gradients lead to increased dislocation density [3]. Dislocation density variation between prints adds another complication during the manufacturing process and may be difficult to model and anticipate. Dislocations can affect ductility, strength, electrical and optical properties [4]. Uncertainty during manufacturing can impact the properties of the printed part, while performance variabilities limit the application of AM parts to critical scenarios.

Sandia National Laboratories is a multimission laboratory managed and operated by National Technology & Engineering Solutions of Sandia, LLC, a wholly owned subsidiary of Honeywell International Inc., for the U.S. Department of Energy's National Nuclear Security Administration under contract DE-NA0003525.

Non-destructive evaluation (NDE) of AM parts could give an indication to the dislocation density and can be used to compare different prints of the same piece. This information would help in the decision making process to accept or reject a printed part. Nonlinear ultrasonic techniques are sensitive to microstructural changes and have been shown to be sensitive to changes in dislocation density [5], but the effectiveness of these techniques in AM has not been fully explored. Second harmonic generation occurs when a sinusoidal wave propagates through a material and its interaction with microstructural features generates waves at the second harmonic of the input. This generation is quantified with the acoustic nonlinearity parameter, β [6].

Nonlinear ultrasonic measurements in this work are made using an air-coupled Rayleigh wave detection setup. Rayleigh waves travel on the surface of an object and allow for a variable propagation distance. Varying the propagation distance can be used to isolate material nonlinearity effects. Unwanted nonlinearity effects created by the measurement equipment will remain constant, while material nonlinearity will increase with propagation distance [7]. An air-coupled receiving transducer allows for easier variation in propagation distance while eliminating inconsistent contact conditions at the receiving end. Linear ultrasonic methods are also explored to compare the effectiveness of the more complex nonlinear techniques in additive materials. A heat treatment regime is prescribed for each specimen to help isolate the microstructural origins of the nonlinearity parameter.

THEORY

Two different measurements are performed in this work, a more complex measurement using nonlinear ultrasound, and a linear ultrasonic technique to judge effectiveness of the nonlinear techniques.

Nonlinear Rayleigh Wave Theory

The second harmonic generation of Rayleigh waves is described by Herrmann et al. [8]. The Rayleigh waves propagating in a solid contain both longitudinal and shear wave. The displacements of these components can be decomposed as in Eq. (1) and (2). The x-axis is defined in the direction of wave propagation (longitudinal) and the z-axis is defined perpendicular to the material (shear).

$$u_x(\omega_o) = B_1\left(e^{-pz} - \frac{2ps}{k_R^2 + s^2}e^{-sz}\right)e^{i(k_R x - \omega t)} \tag{1}$$

$$u_z(\omega_o) = iB_1\frac{p}{k_R}\left(e^{-pz} - \frac{2k_R^2}{k_R^2 + s^2}e^{-sz}\right)e^{i(k_R x - \omega t)} \tag{2}$$

where $p^2 = k_R^2 - k_L^2$ and $s^2 = k_R^2 - k_S^2$; and k_R, k_L , and k_S are the wavenumbers for Rayleigh, longitudinal, and shear waves respectively. Similarly, the Rayleigh waves produced by second harmonic generation can be described at sufficiently large propagation distances from the wedge as

$$u_x(2\omega_o) \approx B_2\left(e^{-2pz} - \frac{2ps}{k_R^2 + s^2}e^{-2sz}\right)e^{2i(k_R x - \omega t)} \tag{3}$$

$$u_z(2\omega_o) = iB_2\frac{p}{k_R}\left(e^{-2pz} - \frac{2k_R^2}{k_R^2 + s^2}e^{-2sz}\right)e^{2i(k_R x - \omega t)}. \tag{4}$$

B_1 and B_2 are the amplitudes of the fundamental and second harmonic waves in the respective equation. In isotropic materials, acoustic nonlinearity arises solely due to the longitudinal wave components (x-axis) because of symmetry conditions [6]. AM materials can display anisotropic behaviors caused by the layer-by-layer building approach [9].

Determining if the symmetry condition holds in the application of nonlinear ultrasonics to AM is a basis for the intellectual curiosity behind this work. Herrmann derived the acoustic nonlinearity parameter, β, from the vertical displacements at the surface (z = 0) for the fundamental and second harmonic waves [8]

$$\beta = \frac{\bar{u}_z(2\omega_o)}{\bar{u}_z^2(\omega_o)x}\frac{8ip}{k_L^2 k_R}\left(1-\frac{2k_R^2}{k_R^2+s^2}\right) \tag{5}$$

where $\bar{u}_z = u_z(z=0)$. From Eq. 5, the following proportionality can be seen

$$\beta \propto \frac{\bar{u}_z(2\omega_o)}{\bar{u}_z^2(\omega_o)x} \tag{6}$$

This relative nonlinear parameter is the metric used in this study. The effects from attenuation and diffraction are assumed to be held constant for all samples as measurement techniques are consistent.

Relative Attenuation Measurement Theory

Relative acoustic attenuation is used as a linear measurement used here to compare the effectiveness of the nonlinear techniques. Like the nonlinear parameter, the attenuation coefficient is sensitive to microstructural changes, and has been used to characterize damage [10]. The wave speed is measured for each specimen and by measuring the time difference between the initial wave packet and the first reflection

$$c = \frac{2\times z}{t_2 - t_1} \tag{7}$$

where z is the sample thickness and t_1 & t_2 are the temporal locations of the same point on two contiguous packets. The magnitude for complex frequency spectra of each packet can be found from [10]

$$s_n(f) = \frac{\lambda \times \Delta x}{b^2} \tag{8}$$

where λ is the wavelength of the signal found using the wave speed in Eq. 7 and the inputted frequency. Δx is total distance travelled by the corresponding wave packet, and b is the radius of the transducer. Equation 8 is used to calculated magnitudes of the complex diffraction correction functions corresponding to the propagation distances of these signals, D, as described by Rogers and Van Buren. [11]

$$D(s_n) = 1 - e^{-i\frac{2\pi}{s_n}}\left[J_o\left[\frac{2\pi}{s_n}\right] + iJ_1\left(\frac{2\pi}{s_n}\right)\right] \tag{9}$$

where J_n is a Bessel function of the first kind of order n. Equation 9 and the voltage ratio between wave packets can be used to calculate the attenuation coefficient

$$\alpha(f) = \frac{1}{2z}\left[\ln\left(\left|\frac{v_1}{v_2}\right|\right) - \ln\left(\left|\frac{D(s_1)}{D(s_2)}\right|\right)\right] \tag{10}$$

In Equation (10), v_1/v_2 is the measured voltage ratio between the steady state portions of the first and second wave packets. This attenuation measurement does not correct for losses between the transducer and material surface;

however, with a consistent experimental setup, the largest contribution to the variation between each specimen's attenuation will come from the material itself. Thus, these values are used as a relative attenuation measurement to compare between the specimens in this work.

SPECIMEN PREPARATION

Four specimens are used in this study. Two are manufactured through additive manufacturing and two through traditional manufacturing techniques; for each manufacturing technique, two stainless steel variants are used, 316L and 304L. The list of specimens is seen in Table 1. The variation in stainless steel comes from the different chemical composition as seen in Table 2. The largest difference between 304 and 316 stainless steels is the higher concentration of molybdenum in 316. All metals used in this study are L variants which indicate a low carbon content defined at <0.04% carbon. The test specimens are flat bars of different dimensions. The thinnest sample is the 316L PBF specimen with a thickness of 1 cm as measured after all surface preparations. The Rayleigh wave displacement is negligible beyond a depth of 1.5λ, where the wavelength λ is approximately 2.64 mm [12]. The Rayleigh wave displacement would be negligible deeper than 0.396 cm; therefore, the wave will propagate without any reflections from the bottom surface. All specimens are initially surface ground to have parallel top and bottom surfaces. Then, they are hand polished to a finish of 1500 grit in order to increase the signal-to-noise ratio (SNR).

TABLE 1. The four specimens and the corresponding manufacturing technique and metal variant are listed

	316L	**304L**
Additive Manufactured	316L PBF	304L LENS
Wrought	316L Wrought	304L Wrought

TABLE 2. Typical chemical composition of stainless alloys in wt.% [13]

Chemical	C	Co	Cr	Cu	Mn	Mo	N	Ni	P
304L	.04	0.17	18.10	0.29	1.25	0.22	.08	8.15	0.03
316L	.02	0.19	16.92	0.28	1.30	2.01	.04	10.38	0.03

Additive Manufacturing Methods

Two different additive manufacturing techniques are investigated in this study. The 316L AM piece is made through a Powder Bed Fusion (PBF) process, while the 304L AM piece is made through Laser Engineered Net Shaping (LENS). PBF is an AM technologies classification defined by the American Society for Testing and Materials (ASTM). Small regions of already deposited bulk material powder are fused with thermal energy applied by either laser or electron beam. Once a layer has been printed, the printing bed will lower and a new layer of fresh powder is placed on top to repeat the process [1].

LENS is a specific technology under the Directed Energy Deposition ASTM classification in which thermal energy is applied during the deposition of the material [14]. A high-power laser is used to heat a substrate onto which a powdered material is then immediately placed. The energy and material inputs are co-located allowing for complex shapes needing spot-by-spot articulation [1].

Heat Treatment

Heat treatments are used in this experiment to cause a change to the dislocation density of the samples and determine the nonlinearity parameters sensitivity to this change. The temperatures and times for the heat treatment roughly follow the heat treatments prescribed by Smith et al. [15]. This annealing profile leads to a decrease in dislocation density as predicted by the decrease of geometrically necessary dislocations (GNDs) observed in the literature [16]. GNDs are part of an interrelated dislocation density formulation along with statistically stored dislocations (SSDs) and grain boundary dislocations (GBDs). GND density correlates to microstructural formation and characterizes the dislocation composition [17]. The final heat treatment for each specimen intends to cause complete recrystallization. Gradual increments towards total recrystallization are taken for finer gradation on the microstructural changes in relation to β measurements. Specimens are either heated in an inert atmospheric oven or in near-vacuum stainless steel bags to prevent oxidization. All specimens are air quenched at room temperature. Specimens are sanded again following the heat treatment process to remove any oxidization which does occur from

trapped atmosphere. This work only presents the measurements before and after the initial heat treatment (HT 1) and shows the immediate effects seen from any application of heat. Future work will be done to explore the effects from the entire heat treatment plan.

TABLE 3. Heat Treatment Plan

Sample	HT 1	HT 2	HT 3	HT 4
304L LENS	1325 K for 0.5 hr	1473 K for 2.5 hr	N/A	N/A
316L PBF	923 K for 0.5 hr	1223 K for 0.5 hr	1323 K for 0.5 hr	1473 K for 2.5 hr
316L Wrought	923 K for 0.5 hr	1223 K for 0.5 hr	1323 K for 0.5 hr	1473 K for 2.5 hr
316L Wrought	1325 K for 0.5 hr	1473 K for 2.5 hr	N/A	N/A

EXPERIMENTAL SETUP

Nonlinear Rayleigh Wave Experimental Setup

The Rayleigh wave setup is shown in the schematic in Fig. 1. A Rayleigh wave is excited with a traditional contact transducer coupled to a wedge. All points of contact between the transducer, wedge, and specimen are coupled with petroleum based oil (PBO). The entire setup is allowed to rest 30 minutes prior to any measurements to reduce any settling effects from the couplant and reduce instrumentation noise. A 2.1 MHz transducer is connected to a function generator to produce a tone burst signal with a peak to peak voltage of 800 mV. 20 cycles are generated with a burst period of 20 ms. A RITEC GA-2500A, a high power gated amplifier, is used to increase the signal-to-noise ratio and leads to better detection of the second harmonics generated in the material. The Rayleigh wave is allowed to propagate along the surface of the specimen; leaked Rayleigh waves are measured by an air coupled transducer connected to a moving stage.

The stage allows for three degrees of translation and one degree of rotation. Before every measurement, the setup is calibrated to find the path of maximum first harmonic amplitude propagation. The angle of the receiving air coupled transducer is calibrated and held constant throughout the measurement. The points of maximum amplitude at the start and end of the set propagation length are found and measurements are made along the connecting path.

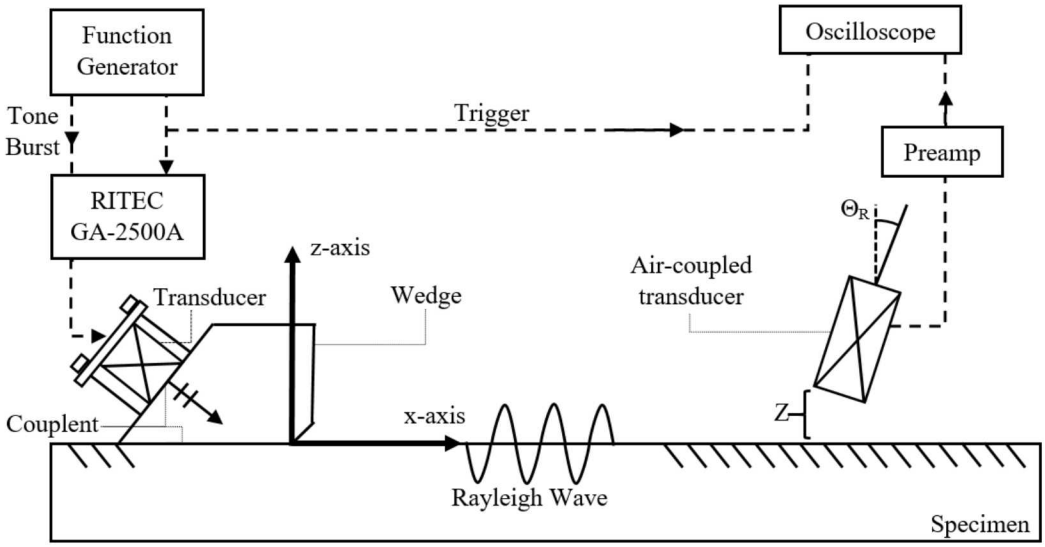

FIGURE 1. Rayleigh surface wave nonlinear ultrasonic measurement setup. Transducer coupled to wedge on left propagates in positive x-direction across specimen surface towards air-coupled transducer. Not shown is stage connected to air-coupled transducer which allows for calibration and variable propagation distance. Dashed lines indicate wiring setup for technical equipment.

The recorded signal is post amplified and averaged 512 times to improve signal-to-noise ratio. A typical time domain signal of this measurement is seen in Fig. 2a. A Hanning window is applied to the signal to reduce the transient effects of voltage overshoot and ringing at the beginning and end of the signal, respectively [7]. A Fast Fourier transform (FFT) transforms the time-domain signal into the frequency spectrum. In Fig. 2b, the frequency spectrum shows the clear distinction between the fundamental, A_1, and second harmonic, A_2. These amplitude values are used to compute the relative nonlinearity parameter β as described in Eq. 6. The relation between A_1 and A_2 are studied over the propagation distance and are seen in Fig. 3. The value for β is found from the slope of the ratio in Fig. 4. The nonlinearity parameter is a relative measurement used to study the change occurring within the specimen, therefore the values are normalized to the lowest recorded β for the data set.

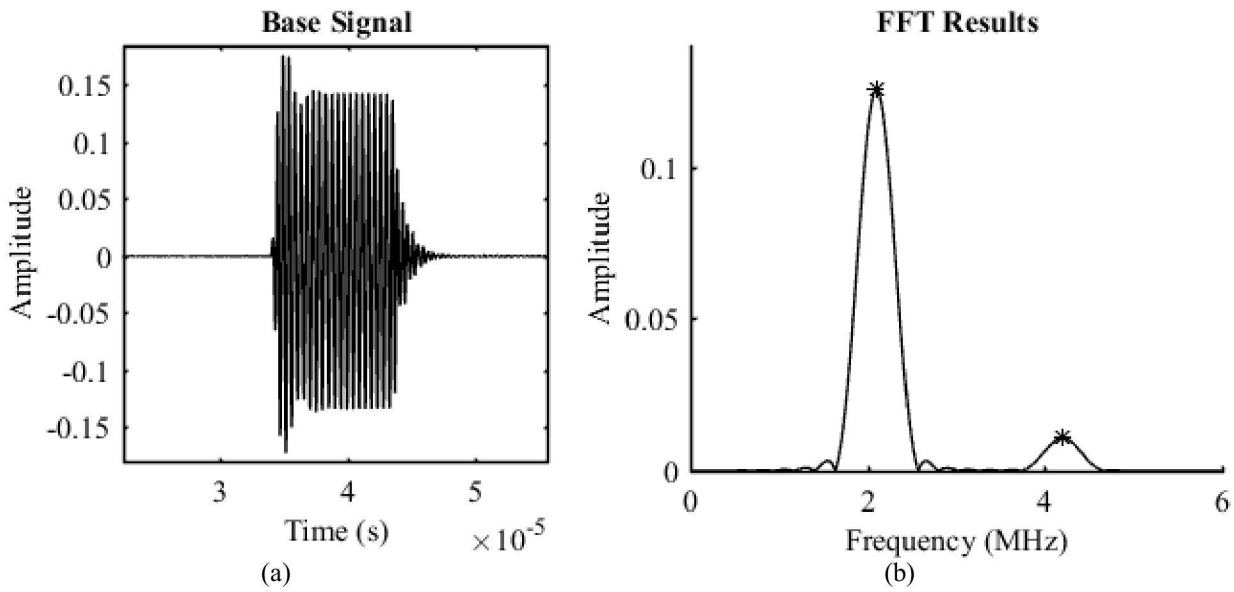

FIGURE 2. (a) Time averaged base signal measured from air coupled transducer includes transient regions. Y axis indicates oscilloscope reading of voltage (b) FFT results after windowing shows separation of fundamental frequency at 2.1 MHz and second harmonic at 4.2 MHz.

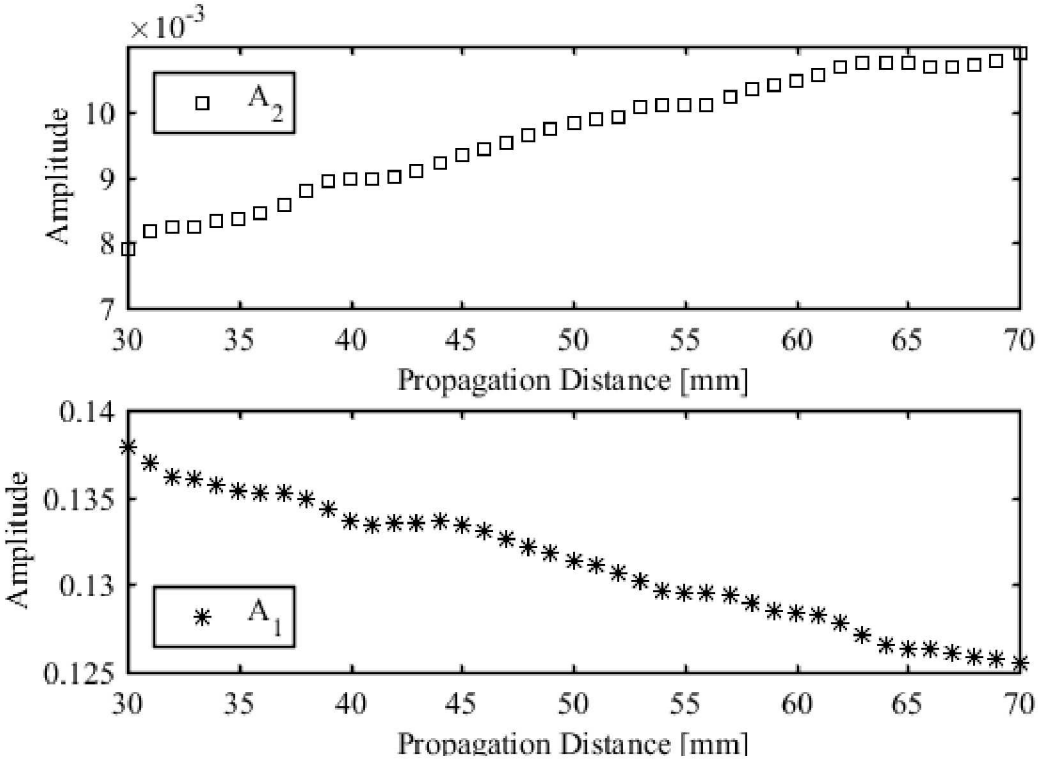

FIGURE 3. A_2 and A_1 versus propagation distance

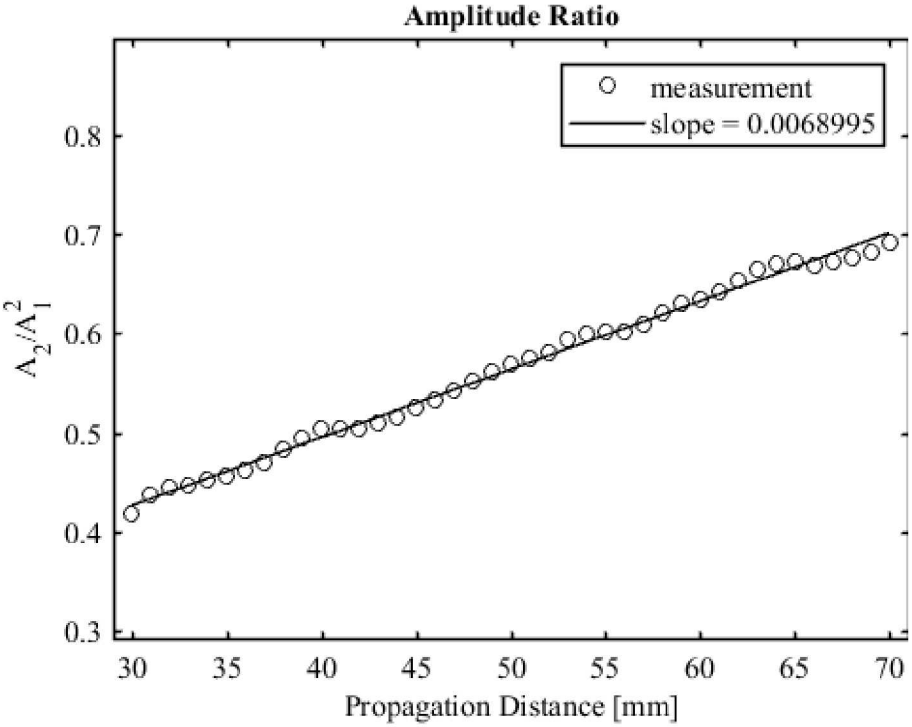

FIGURE 4. Example ratio of A_2/A_a^2 plotted over propagation distance. The nonlinearity parameter for one measurement is found from slope of this plot.

Relative Attenuation Experimental Setup

The attenuation for each specimen is measured using contact transducers in a through transmission setup as seen in Fig. 5. Two ultrasonic transducers, one transmitting and one receiving, are clamped through the thickness of the material with an oil based couplant between each contact surface. Two wave packets are examined for each measurement; the first signal (labeled 1 in Fig. 5) travels through the thickness of the specimen once, while the second (labeled 2 in Fig. 5) travels through the sample three times. For each measurement, the attenuation coefficient is measured for a sweep of frequencies from 8 MHz to 20 MHz, changing the wavelength seen in Eq. 8. The trend of attenuation as a function of frequency is then compared between each sample and heat treatment state.

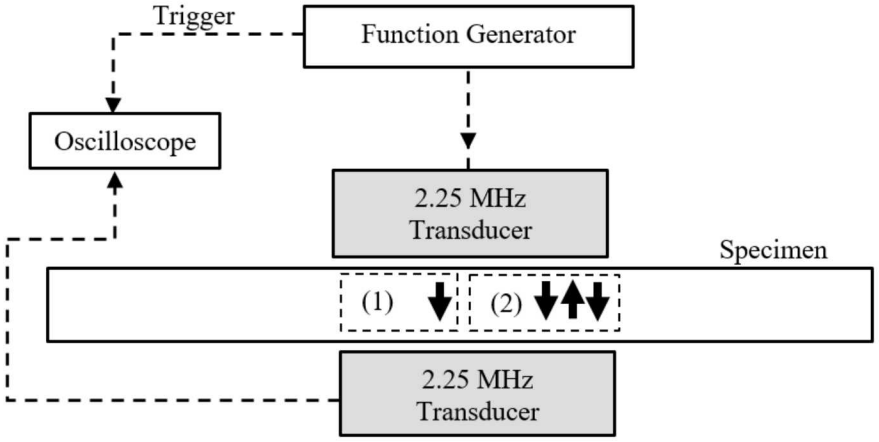

FIGURE 5. Through transmission attenuation measurement setup. Dashed boxes labeled 1 & 2 in specimen show path taken from first and second wave packet.

RESULTS AND DISCUSSION

Rayleigh wave measurements are performed for each sample before and after the first stage of their heat treatment plan. The results are plotted in Fig. 6. The nonlinearity parameter β is normalized to the lowest value measured from the set of specimens, as only the relative differences between the measurements are of importance. Each boxplot is composed of five measurements. For each specimen, the measurements before and after heat treatment (annealing) are placed next to each other showing the β decrease in each sample following heat treatment. β was hypothesized to decrease after the heat treatment as it was predicted to be an increasing function of dislocation density [5]. When comparing across specimens in both the untreated and heat-treated states, β is higher for both samples produced by AM. High temperature gradients contribute to the chaotic microstructural environment resulting from the AM process [15]. The building environment likely contributes to an increase in dislocation density that is quantified in β.

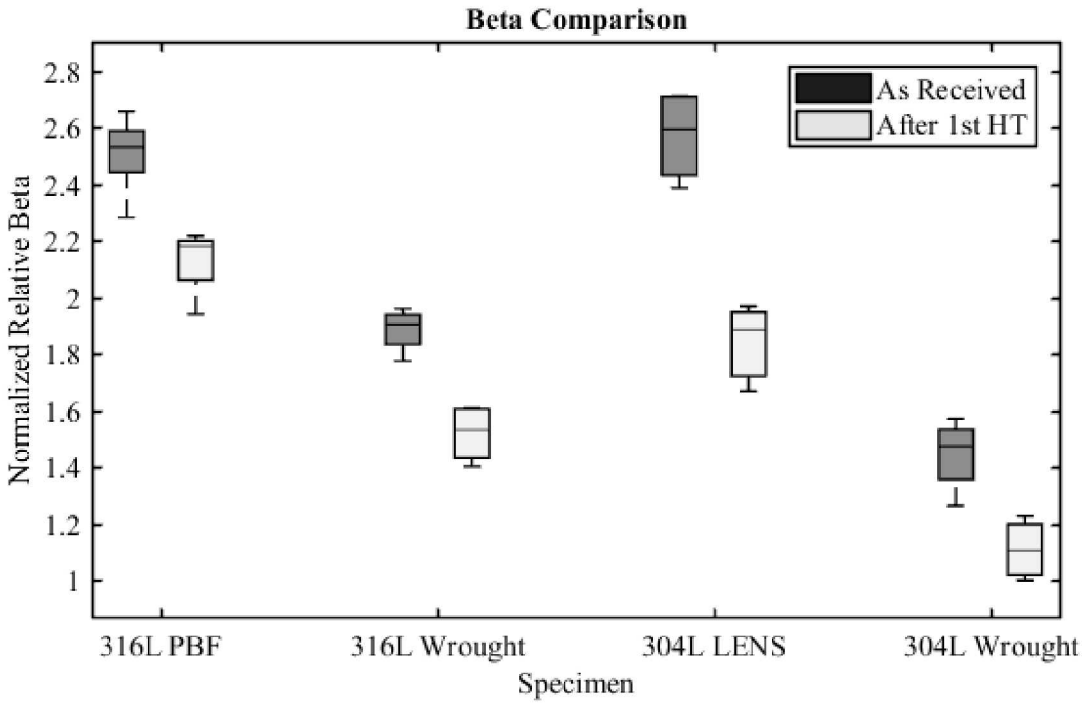

FIGURE 6. A comparative box plot chart for the normalized β values for each specimen before (dark shaded box) and after (light shaded box) the first heat treatment is performed. Each box plot represents five nonlinearity measurements performed.

Attenuation measurements are also performed for each sample before and after the first stage of their heat treatment plan. The results are plotted as a function of frequency in Fig. 7. Measurements for 304L LENS following heat treatment were not completed by the time of this work. Attenuation increases following heat treatment at higher frequencies. The sensitivity of the measurement techniques may not show the separation at lower frequencies for a specimen before and after heat treatment. Annealing leads to higher relative attenuation potentially due to an increase in grain size. The ratio of grain size to ultrasonic wavelength has been shown to affect the scattering regimes of ultrasonic waves [18,19]. AM parts have significantly higher attenuations which is consistent with their more complex microstructure [20]. The complex microstructure comes from the multi-component nature of the base alloys, and the temperature gradients of the printing process [21]. Metallic AM often contains microstructural features that are rarely seen in wrought manufactured metals [21].

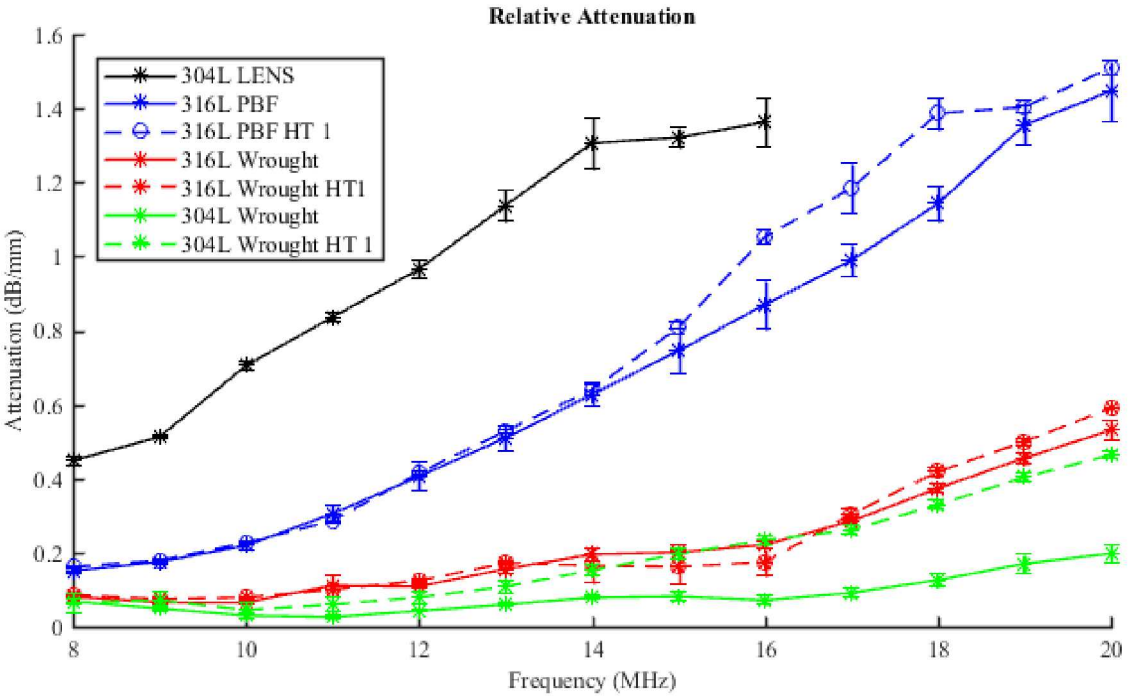

FIGURE 7. Relative attenuation values plotted versus the frequency. Dotted lines of the same color indicate attenuation after first prescribed heat treatment. Each symbol represents average of five measurements.

CONCLUSION

The nonlinear acoustic parameter shows high sensitivity to the predicted changes in dislocation density in additive manufactured materials. Similarly, the linear ultrasonic attenuation also shows sensitivity to these changes at high frequencies. Comparisons between the effectiveness of the two measurements will be made once all measurements are completed. Continuation of this work will include finishing the cycle of measurements and heat treatments (gradual annealing) until total recrystallization occurs. Microstructural changes will be investigated through metallurgical analysis at each stage of the heat treatment cycle.

ACKNOWLEDGMENTS

Financial support and materials for this research are provided by Sandia National Laboratories. Sandia National Laboratories is a multimission laboratory managed and operated by National Technology and Engineering Solutions of Sandia, LLC, a wholly owned subsidiary of Honeywell International, Inc., for the U.S. Department of Energy's National Nuclear Security Administration under contract DE-NA-0003525. SAND 2018-xxxxC.

REFERENCES

1. L. Yang, K. Hsu, B. Baughman, D. Godfrey, F. Medina, M. Menon, and S. Wiener, *Additive Manufacturing of Metals: the Technology, Materials, Design and Production* (Springer, Cham, 2017), p. 5
2. Y. Kok, X.P. Tan, P.Wang, M.L.S Nai, N.H. Loh, E. Liu, S.B. Tor, Materials and Design 139, 565 (2018)
3. S. Gorsse, C. Hutchinson, M. Gouné, and R. Banerjee, Science and Technology of Advanced Materials **18**, 584 (2017).
4. D.R. Askeland, P.P. Phule, and W.J. Wright, *The Science and Engineering of Materials: Sixth Edition*(Cengage Learning, Mason, OH, 2011).
5. A. Hikata, B. B. Chick, and C. Elbaum, J. Appl. Phys. 36(1), 229 (1965)
6. K.H. Matlack, J.-Y. Kim, L.J. Jacobs, and J. Qu, Journal of Nondestructive Evaluation **34**, (2014).
7. S. Thiele, J.-Y. Kim, J. Qu, and L.J. Jacobs, Ultrasonics **54**, 1470 (2014).
8. J. Herrmann, J.-Y. Kim, L. Jacobs, and J. Qu, Journal of Applied Physics 99, p 124913 (2006)
9. N. Shamsaei, A. Yadollahi, L. Bian, and S.M. Thompson, Additive Manufacturing **8**, 12 (2015).
10. M. Treiber, J.-Y. Kim, L.J. Jacobs, and J. Qu, The Journal of the Acoustical Society of America **125**, 2946 (2009).
11. P.H. Rogers and A.L.V. Buren, The Journal of the Acoustical Society of America **55**, 724 (1974).
12. D.T. Zeitvogel, K.H. Matlack, J.-Y. Kim, L.J. Jacobs, P.M. Singh, and J. Qu, NDT & E International (2013)
13. Rokosz, J. Lahtinen, T. Hryniewicz, and S. Rzadkiewicz, Surface and Coatings Technology 276, 516 (2015).
14. S.M. Thompson, L. Bian, N. Shamsaei, and A. Yadollahi, Additive Manufacturing **8**, 36 (2015).
15. T.R. Smith, J.D. Sugar, J.M. Schoenung, and C.S. Marchi, Jom **70**, 358 (2018).
16. D. Susan, D. Kammler, C. Profazi, C. Taylor, A. Roach, B. Boyce, J.P. Lopez, and R. Andersen, Additive Manufacturing JOWOG (2017).
17. O. Rezvanian, M. Zikry, and A. Rajendran, Proceedings of the Royal Society A: Mathematical, Physical and Engineering Sciences **463**, 2833 (2007).
18. T. Wan, T. Naoe, T. Wakui, M. Futakawa, H. Obayashi, and T. Sasa, Materials **10**, 753 (2017).
19. A. Van Pamel, P.B. Nagy, and M.J.S. Lowe, The Journal of the Acoustical Society of America **140**, 4360 (2016).
20. K. Makiewicz, M. Keller, A.B. Chaudhary, and S.S. Babu, 9th International Conference on Trends in Welding Research American Society for Metals (2012).
21. Y. Ji, L. Chen, and L.-Q. Chen, in *Thermo-Mechanical Modeling of Additive Manufacturing* (Butterworth-Heinemann, 2018), pp. 93–116.